Linear velocity spectrum (Thesis chapter IV)

Alfonso González-Serrano
Jon F. Claerbout

Abstract

The wave equation velocity spectrum of a CMP is defined as its image in Snell midpoint coordinates for a non–zero reference ray parameter p_0. In this space energy is a local function of velocity. Velocity estimation is possible with the LMO method. In stratified media with constant velocity between reflectors, the LMO method estimates interval velocity without the need of geometric approximations. The LMO method can also be used to quantify strong velocity variations between reflectors. The phase shift method is a convenient way to downward continue in Snell midpoint coordinates. Stolt's method can be combined with a hyperbolic deformation to improve the quality of imaging. Because downward continuation operators are referenced to a slant propagation angle, accurate operators to image wide angle energy are unnecessary. The fifteen degree finite difference method in (h, τ, ω) can thus be used at wide angles. This method is not too sensitive to the downward continuation velocity. A variable velocity $v(h, \tau)$ can be used to improve the image. Also we can apply a stepout filter concurrent with downward continuation. Examples with synthetic and field data show that the linear velocity spectrum can resolve both narrow and wide velocity variations when using the appropriate reference parameters. The wave equation velocity spectrum is also a convenient model space when linearity and locality properties are desired.

1. Introduction. Velocity space.

The acoustic wave equation has been successfully applied to the migration problem in reflection seismology. For the velocity estimation problem, however, the wave equation has received limited attention. Wave equation methods have the important attribute of linearity, a property not found in commonly used ray tracing techniques. In this chapter our goal is to

define a *velocity spectrum* of CMP gathers using wave equation techniques.

We require the velocity spectrum to have two fundamental properties. 1) It must be a space where energy from different events is a local function of velocity. 2) The space must be defined by invertible transformations. Two other desirable properties are resolution and accuracy.

Ray methods are commonly used to estimate velocity. Their application results in non-linear transformations on the data. An alternative method of velocity estimation is the *linear moveout method.* An important and elegant feature of this method is that it follows directly from the Snell midpoint coordinate transformation. This method is the most natural choice for implementation with the wave equation.

The linear moveout method estimates velocity using the lateral component of a reference Snell wavefront. We can measure either RMS or interval velocities directly in the data. In a stratified earth, with reflectors coinciding with velocity discontinuities, interval velocity can be measured at any angle, no geometric approximations need to be done. RMS velocity estimates as defined with Dix's equation can also be determined. With this method we can use wide angle reflections for direct interval velocity estimation. When there are continuous velocity variations between reflectors, reflection traveltime data alone cannot resolve uniquely for the velocity function. The problem is underdetermined. Snell coordinates can then be used to decide when velocity inhomogeneities between reflectors are not negligible.

The LMO method does not define a suitable velocity space. Adding an imaging step, however, makes energy become a local function of velocity. Imaged data in Snell midpoint coordinates will constitute our definition of the linear velocity spectrum. Given that imaging will be needed to transform to our velocity space, we describe three methods to image CMP gathers in Snell midpoint coordinates. First, the phase shift method, which is particularly useful to study downward continuation problems. Second is Stolt's method, which is the fastest and can be complemented with a hyperbolic deformation. And last, finite difference in (h, τ, ω) space, which allows us to use $v(h,\tau)$ in the downward continuation and do stepout filtering concurrent with imaging. Snell midpoint coordinates enable us to use low order wave equation operators for wide propagation angles. This and the insensitivity of the fifteen degree equation to the background velocity, makes the finite difference method the preferred choice to obtain the velocity spectrum.

The wave equation velocity spectrum can also be used in applications requiring model spaces with linearity and locality properties.

2. Ray methods in velocity estimation.

Ray methods can be applied in several domains. In this section only methods in the (h, τ, t) domain will be considered.

All ray tracing techniques for velocity estimation are based on the asymptotic high frequency approximate solution of the wave equation. In a flat earth, travel-time as function of offset for the n^{th} arrival is given by

$$t_n^2(h) \approx t_{0,n}^2 + \frac{4h^2}{v_{RMS,n}^2} + O(h^4) \tag{2.1}$$

where h is half offset, t_0 the vertical traveltime and v_{RMS} the Root Mean Square velocity.

Green (1938) was the first to use this equation to estimate velocity. Plotting $4h^2$ *vs* t^2 gives straight lines with intercept $t_{0,n}^2$ and slope $1/v_{RMS,n}^2$. To find interval velocities, Dix (1955) derived a relationship using v_{RMS}

$$v_n^2 = \frac{v_{RMS,n}^2 \sum_1^n \Delta t_{0,i} - v_{RMS,n-1}^2 \sum_1^{n-1} \Delta t_{0,i}}{\Delta t_{0,n}} \tag{2.2}$$

This equation is widely used. Hajnal and Serada (1981) give a quantitative discussion of errors in interval velocities computed from Dix's equation. In particular, interval velocity estimates amplify RMS velocity errors, and are oversensitive to errors in the normal incidence traveltime estimates.

LePichon *et al* (1968) proposes a least–square fit to equation (2.1). His approach is convenient whenever arrival times for particular events can be picked out automatically. Unfortunately, automatic picking is unreliable in low amplitude signal environments. The method is limited by the signal–to–noise ratio of the data.

The most widely accepted method for defining velocity spectrum is Taner and Koehler's (1969) technique. They use equation (2.1) to apply a correction for residual travel time with offset, (*NMO* correction):

$$t_n(h) - t_{0,n} \equiv \Delta t_n(h) \approx \frac{h^2}{2v_{RMS,n}^2 t_0} \tag{2.3}$$

After NMO, first arrival traveltimes should be independent of offset (approximately if the velocity is not constant). The correction is applied for a trial set of velocities. For display some semblance measure can be used (Neidell and Taner, 1971; Taner and Koehler, 1968). Figure (2.1) is an example of this technique. Unless refractions are muted out and primary energy is kept to small propagation angles, the velocity spectrum does not give good resolution.

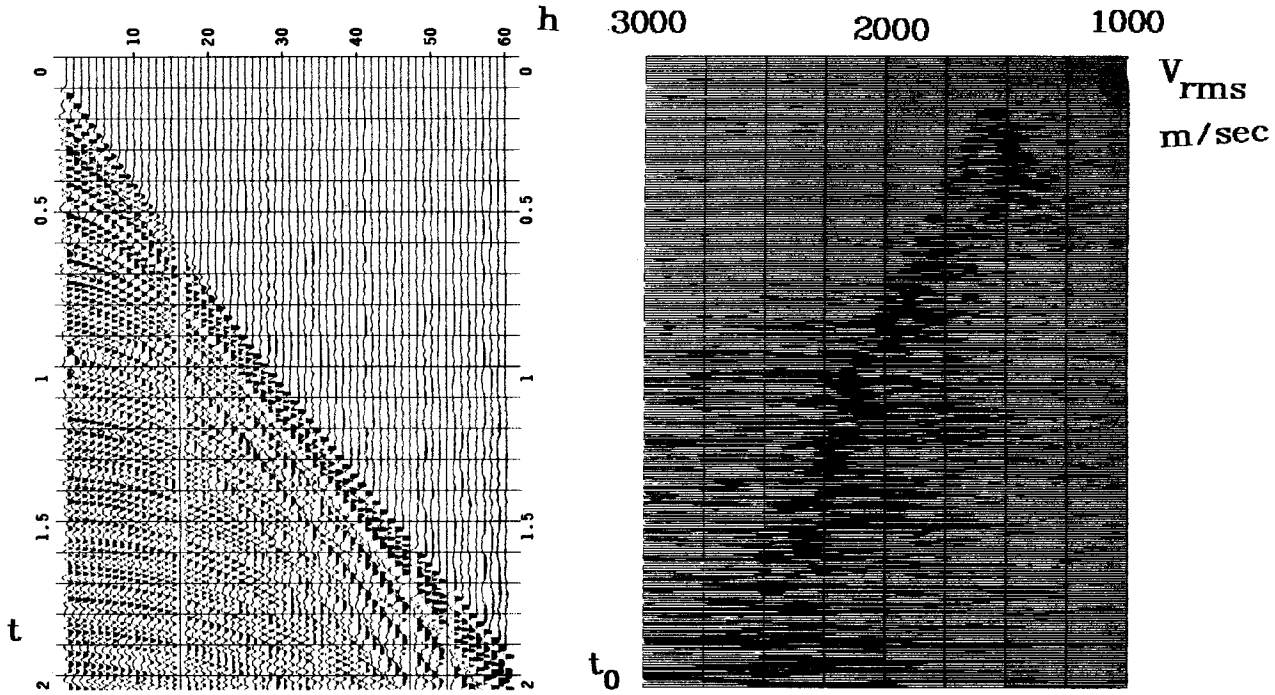

FIG. 2.1. Hyperbolic velocity spectrum. (a) CMP gather. (b) Hyperbolic velocity spectrum. Note in particular the poor resolution for the first 350 ms of data because refractions were not muted out.

May and Straley (1979), include the fourth order term in equation (2.1). This term gives a first order correction to non–hyperbolicity. The truncated series needs to be orthogonalized before estimating its coefficients. Since there are three coefficients, (zero, second and fourth order), a coherence search needs to be done in 3–D space. They suggest two searches over 2–D planes, implying hyperbolic assumption in one plane. This method is particularly useful as a processing tool, to improve the NMO correction with better stacking velocities.

The ray methods discussed above have the advantage of insensitivity to aliasing. However, they have several important restrictions. First, they are approximations dependent on angle. Error increases with offset where the data is most sensitive to velocity. Second, ray methods are non–linear; and third, their resolution is limited by cable truncations and refractions. In the next section we reconsider these limitations with the LMO method.

3. Linear moveout method.

Claerbout (1980) introduced a direct velocity estimation procedure using Snell waves. The method is a direct consequence of Snell midpoint coordinates at the image point. In this method velocity is determined as a function of arrivals associated with a slanted reference wavefront. In a stratified earth this treatment is exact for all non–offsets. The method requires data in Snell midpoint coordinates. At the surface of the earth ($z = 0$) the Snell coordinates are: (SEP 15, p. 81–87.)

$$t' = t - p_0(g - s) \tag{3.1a}$$

$$y = \frac{g + s}{2} \tag{3.1b}$$

$$h = \frac{g - s}{2} \tag{3.1c}$$

$$\tau = 0 \tag{3.1d}$$

The data, therefore, needs to be sorted into midpoint–offset coordinates. Time should be modified with (equation 3.1a). This correction is commonly referred as *linear moveout correction (LMO)* to distinguish it from the Normal moveout *NMO* dynamic correction. This method of estimating velocity will be referred as the *LMO* method from now on.

Snell midpoint coordinates describe the wave propagation of a slanted reference wavefront. It follows that the lateral coordinate of the wavefront preserves velocity information of the data, independent of the depth of observation. To see this, insert the imaging conditions $s = g$ and $t = 0$ in the definitions of Snell coordinates to get at fixed midpoint

$$t' = \tau \tag{3.2a}$$

$$h = \int_0^z \frac{p_0 v(\xi)}{[1 - p_0^2 v(\xi)^2]^{1/2}} d\xi \tag{3.2b}$$

$$\tau = 2 \int_0^z \frac{[1 - p_0^2 v(\xi)^2]^{1/2}}{v(\xi)} d\xi \tag{3.2c}$$

With $\frac{dh}{dz}$ and $\frac{d\tau}{dz}$ we can use the chain rule to eliminate dz and solve for velocity:

$$v^2 = \frac{1}{p_0 \left[p_0 + \frac{1}{2} \frac{d\tau}{dh} \right]} \tag{3.3}$$

When the reference ray parameter is zero, this equation is indeterminate, implying velocity information is not available at at zero offset. Equation (3.3) is valid at any depth of

observation.

Using equation (3.3) we can estimate velocity directly from the data. The ray parameter p_0 fixes the departure angle of the reference wavefront. The slope $\frac{d\tau}{dh}$ is measurable directly from the data. We consider two alternatives to measure this slope. It can be measured from the origin, or it can be measured between two consecutive primary arrivals. What velocity is being measured?.

First notice that the slanted time τ_0 is not equal to the vertical time t_0; a cosine correction needs to be done. Assuming velocity can be parameterized in different variables

$$v(z) = v_\tau(\tau(z)) = v_t(t(z))$$

$$\vartheta(z) = \vartheta_\tau(\tau(z)) = \vartheta_t(t(z))$$

The observed τ_0 in slanted coordinates is given by

$$\tau_0 = 2\int_0^z \frac{[1 - p_0^2 v^2(\xi)]^{1/2}}{v(\xi)} d\xi \tag{3.4}$$

while the vertical traveltime is

$$t_0 = 2\int_0^z \frac{1}{v(\xi)} d\xi \tag{3.5}$$

Combining equations (3.4) and (3.5) yields

$$\tau_0 = \int_0^{t_0} [1 - p_0^2 v_t^2(\xi)]^{1/2} d\xi \tag{3.6}$$

$$t_0 = \int_0^{\tau_0} \frac{1}{[1 - p_0^2 v_\tau^2(\xi)]^{1/2}} d\xi \tag{3.7}$$

or, approximating the propagation angle to a constant $\cos\bar{\vartheta}_0 = [1 - p_0^2\bar{v}^2]^{1/2}$,

$$t_0 = \frac{\tau_0}{\cos\bar{\vartheta}_0} \tag{3.8}$$

If t_0 is not picked directly from the data, this equation shows how to find it from the image positions τ_0. The depth is given by

$$z = \frac{1}{2}\int_0^{\tau_0} \frac{v_\tau(\xi)}{[1 - p_0^2 v_\tau^2(\xi)]^{1/2}} d\xi = \frac{1}{2}\int_0^{t_0} v_t(\xi)\, d\xi \tag{3.9}$$

To find what velocity the LMO method measures, by combining equations (3.2) and (3.6) we can write the arrival offset h as a function of τ

$$h = \frac{1}{2}\int_0^\tau \frac{p_0 v_\tau(\xi)^2}{1 - p_0^2 v_\tau(\xi)^2}\, d\xi$$

or since $\cos^2\vartheta_\tau = 1 - p_0^2 v_\tau^2$

$$h = \frac{1}{2} p_0 \int_0^\tau \frac{v_\tau(\xi)^2}{\cos^2\vartheta_\tau(\xi)}\, d\xi \tag{3.10}$$

We can think of replacing the velocity structure in stratified media by a single layer with constant velocity $\bar{v}$. This statistically represents the velocity structure of the rock column. Replacing $\bar{v}$ in equation (3.10) gives*

$$h = \frac{1}{2}\frac{p_0 \bar{v}^2 \tau}{\cos^2\bar{\vartheta}} \tag{3.11}$$

Solving for $\bar{v}^2$

$$\bar{v}^2 = 2\,\frac{\cos^2\bar{\vartheta}}{p_0}\,\frac{h}{\tau} \tag{3.12}$$

replacing h by the expression of equation (3.10) yields

$$\frac{\bar{v}^2}{\cos^2\bar{\vartheta}} = \frac{1}{\tau}\int_0^\tau \frac{v_\tau(\xi)^2}{\cos^2\vartheta_\tau(\xi)}\, d\xi \tag{3.13}$$

We can rewrite this equation as function of the two–way traveltime t

$$t = \int_0^\tau \frac{1}{\cos^2\vartheta_t(\xi)}\, d\xi \equiv \frac{\tau}{\cos^2\bar{\vartheta}} \tag{3.14}$$

to obtain

$$\bar{v}^2 = \frac{1}{t}\int_0^t v_t(\xi, p_0)^2\, d\xi \equiv v_{RMS}^2(p_0) \tag{3.15}$$

This is Dix's equation. Constant velocity $\bar{v}$ in equations (3.2b) and (3.2c) give the relation

$$\bar{v}^2 = \frac{1}{p_0\left(p_0 + \frac{1}{2}\frac{\tau}{h}\right)} \tag{3.16}$$

*Since h and τ are fixed, errors in this approximation will affect the depth z.

Therefore, the slope τ/h from the origin gives an estimate of the RMS velocity. This v_{RMS} is not unique, it depends on angle.

Instead, if we measure the slope between two consecutive primary events, from equation (3.2) we have

$$\Delta h = h_{i+1} - h_i = \frac{1}{2} p_0 \int_{\tau_i}^{\tau_{i+1}} \frac{v_\tau(\xi)^2}{\cos^2 \vartheta_\tau(\xi)} d\xi \tag{3.17}$$

Assuming constant *interval* velocity between the events and solving for velocity, we get

$$v^2_{interval} = \frac{1}{p_0 \left[p_0 + \frac{1}{2} \frac{\Delta\tau}{\Delta h} \right]} \tag{3.18}$$

Therefore, when velocity remains constant between any two consecutive primary arrivals, equation (3.3) gives their interval velocity. When velocity varies appreciably between reflectors, interval velocity is unresolved with reflection traveltime data alone. Equation (3.3) gives then a local RMS velocity estimate for the particular choice of p_0. In the next section we analyze this situation.

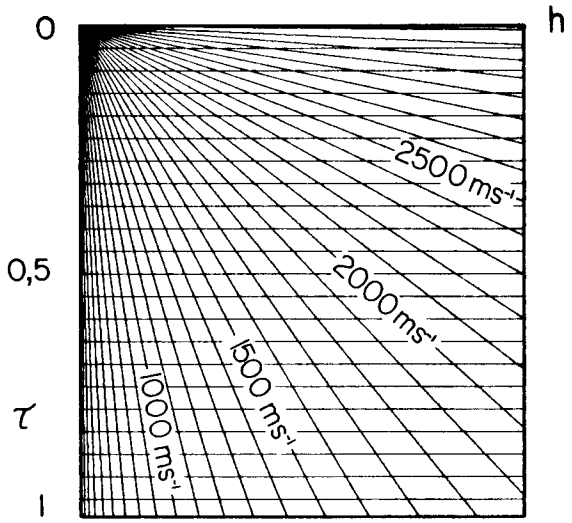

FIG. 3.1. Velocity estimation grid. This grid is a tabulation of equation (3.3) for a fixed value of Snell's parameter p_0. The slope from the origin gives the *RMS velocity*, the slope between two consecutive primary events gives their *Interval velocity*.

It is emphasized that in obtaining equations (3.3) and (3.18) no geometrical approximations were made. The horizontal coordinate of the wavefront has velocity information and these relationships show how to find it. A convenient way of measuring velocity is to tabulate equation (3.3) for a fixed value of the ray parameter p_0. This is shown in figure (3.1).

As pointed out by Schultz (1981), more accurate interval velocity estimates should be used as an interpretation tool more than as a processing tool. Accurate interval velocities do not necessarily imply better stacking velocities. They do imply better migration velocities.

When there is a geologic dip component with angle α, Levin (1971) proved that v_{NMO} obtained using Taner and Koehler's method is v_{RMS} modified by the cosine of the dip angle

$$v_{NMO} = \frac{v_{RMS}}{\cos \alpha} \tag{3.19}$$

This result is valid when slanted reference waves are used.

The LMO has important advantages over ray tracing methods. This method can be used in the far offsets where data has more velocity resolution. The method is flexible in that we can select a value of p_0 where the signal–to–noise ratio of the data is particularly good. Transformation to Snell midpoint coordinates is linear. Also there is more control in deciding what events to use in the velocity estimation process. Multiple reflections preserve their timing relationships, becoming easier to discriminate against primaries. This method is also partially insensitive to refractions and cable truncations. However, the method itself does not define a suitable velocity spectrum; energy remains non–local. In section (5) we approach this problem using the wave equation to image the data in Snell midpoint coordinates.

4. Non–uniqueness of velocity estimates.

In the last section we proved that in stratified earth with flat reflectors and no velocity variations between reflectors, the LMO method could be used to get consistent interval velocity estimates at any propagation angle. The LMO method can also estimate RMS velocities according to Dix's equation.

When there are velocity variations between reflectors, reflection data alone cannot give unique velocity estimates. The problem is underdetermined. This may happen either when there are continuous velocity inhomogeneities between reflectors (infinite unknowns), or if the interval velocity is measured between non–consecutive primary arrivals.

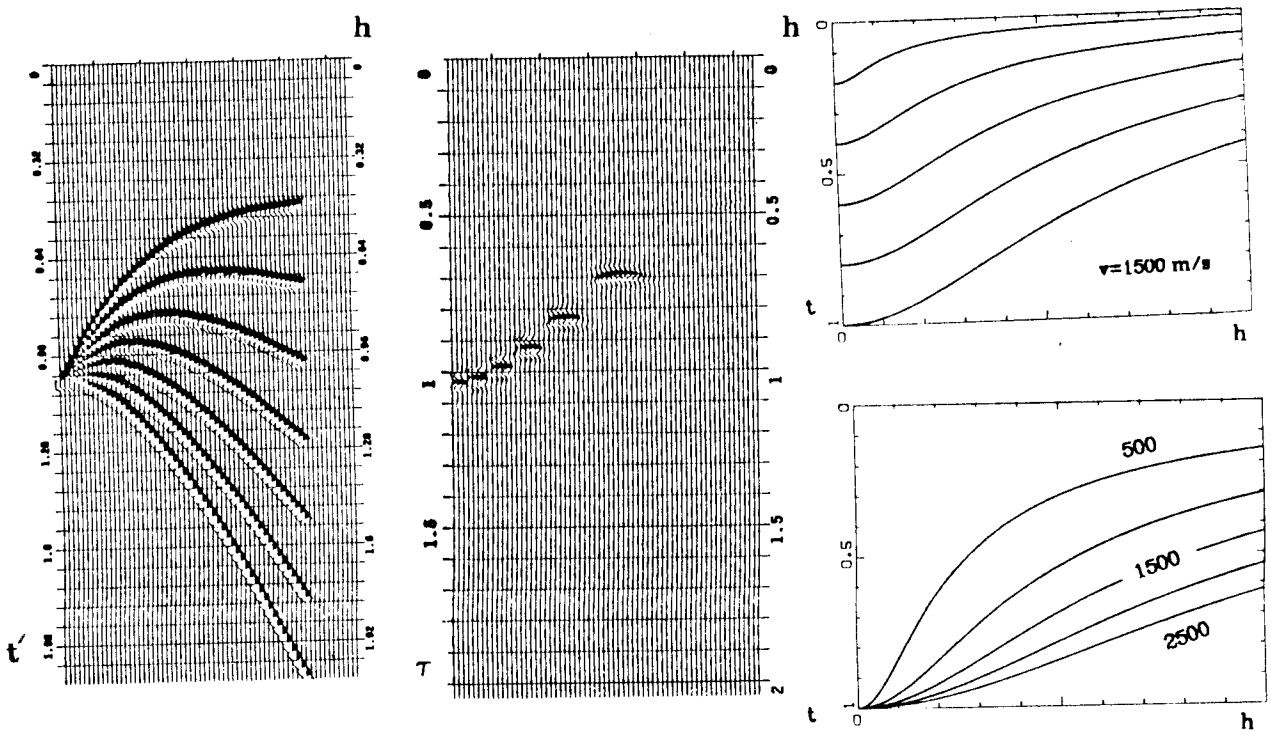

FIG. 4.1. (a) Superposition of synthetic CMP gathers. A LMO correction has been applied with different p_0 before superposition for display. Reference event has $v = 1500\ m/sec$. (b) Imaged CMP gathers. In this diagram it is easy to follow the trajectory of the reference Snell wave arrivals for different p_0. (c) τ_0 *vs* h diagram. This trajectory will be followed by reference Snell wavefronts arrivals with increasing ray parameter p_0. Velocity is constant, different time-depths. (d) Same as (c) with variable velocity and fixed time-depth. The range of offsets is 1575 m, time is in seconds.

The LMO method is sensitive to velocity variations between reflectors. We can use Snell midpoint coordinates to find criteria to decide when these velocity inhomogeneities are not negligible. If this is the case, velocity estimation methods with refraction data, such as the wavefield continuation method of Clayton and McMechan (1981) or the tau-sum inversion method of Diebold and Stoffa (1981), should give better velocity estimates. Refraction methods, however, do not detect velocity reversals.

Reconsidering the question of what velocity the LMO method measures; from equations (3.17) and (3.18) we know that if the velocity remains constant between any two reflectors, then the interval velocity estimate is independent of the reference p_0. If we measure interval velocity at any two locations p_1 and p_2, then

$$1 = \frac{p_1 \left(p_1 + \frac{1}{2} \frac{\Delta\tau}{\Delta h} \Big| p_1 \right)}{p_2 \left(p_2 + \frac{1}{2} \frac{\Delta\tau}{\Delta h} \Big| p_2 \right)} \tag{4.1}$$

As velocity inhomogeneities between reflectors increase, the concept of interval velocity becomes meaningless. To see this, from equation (3.13) we have

$$\frac{\bar{v}^2}{\cos^2\bar{\vartheta}} = \frac{1}{\tau_{i+1}(p_0) - \tau_i(p_0)} \int_{\tau_i(p_0)}^{\tau_{i+1}(p_0)} \frac{v_\tau(\xi)^2}{\cos^2\vartheta_\tau(\xi)} d\xi \tag{4.2}$$

i.e. interval velocity measurements become local angle–dependent RMS velocity estimates.

With equation (4.2) we can quantify whether velocity variations are negligible or not. Defining an error function $\varepsilon(p_1,p_2)$ as

$$\varepsilon(p_1,p_2) \equiv 1 - \frac{p_1 \left(p_1 + \frac{1}{2} \frac{\Delta\tau}{\Delta h} \Big| p_1 \right)}{p_2 \left(p_2 + \frac{1}{2} \frac{\Delta\tau}{\Delta h} \Big| p_2 \right)} \tag{4.3}$$

With ε we can quantify when the interval velocity estimates show angle variations above the measurement uncertainties. That could show there are strong velocity variations between reflectors. A convenient way to test this is to plot the expected *vs* the observed image locations as function of p_0 in the (h,τ) plane. (Figure 4.1)

5. Imaging CMP gathers in Snell midpoint coordinates.

In section (3) we learned that slant wave propagation preserves the velocity information of the data at any depth. Slant downward continuation and imaging does not alter the velocity information of the data. In this section we describe imaging CMP gathers in Snell midpoint coordinates. Given a fixed reference Snell wave, imaging localizes energy to the neighborhood of its corresponding arrival offset.

The double square root equation in Snell midpoint coordinates under the stratified flat reflectors assumption ($Y = 0$), is given by (figure 5.1)

$$T \equiv \frac{k_\tau}{\omega} = 1 - \frac{p_0 v}{1 - p_0^2 v^2} H - \left[1 - \frac{2 p_0 v H + H^2}{1 - p_0^2 v^2} \right]^{1/2} \tag{5.1}$$

$$H = \frac{k_h v}{2\omega}$$

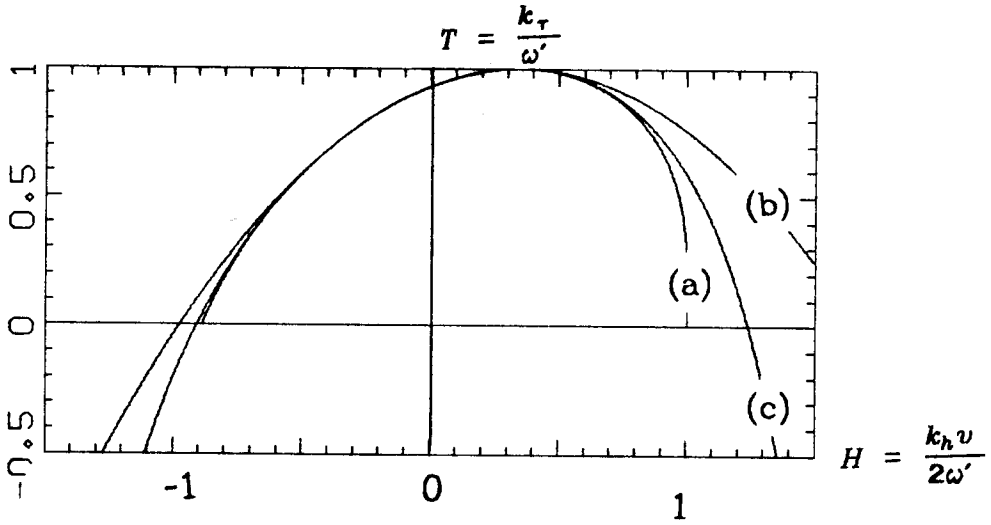

FIG. 5.1. Slant dispersion relation. Square root equation in Snell midpoint coordinates. $Y = 0, p_0 v = 0.3$ (a) Exact equation; (b) Fifteen degree approximation; and (c) Forty–five degree approximation.

To image CMP gathers, first we need to put the data from field coordinates $(s, g, t, z=0)$ into Snell midpoint coordinates $(h, y, \tau=0, t')$. The operator (5.1) is defined in the ω–k domain, so we need to Fourier transform the data $f(y, h, \tau=0, t')$. Omitting the y dependence gives

$$F(k_h, \tau=0, \omega) \;=\; \int_{-\infty}^{\infty}\int f(h, \tau=0, t')\, e^{-ik_h h + i\omega t'}\, dh\, dt'$$

using equation (5.1) the data at any time–depth τ is given by

$$F(k_h, \tau, \omega) \;=\; F(k_h, \tau=0, \omega) \exp\left\{ i \int_0^{\tau} T(\xi)\, \omega\, d\xi \right\} \tag{5.3}$$

Fourier transforming back to (h, τ, t') space

$$f(h, \tau, t') \;=\; \frac{1}{4\pi^2} \int_{-\infty}^{\infty}\int F(k_h, \tau=0, \omega) \exp\left\{ i \int_0^{\tau} T(\xi)\, \omega\, d\xi + ik_h h - i\omega t' \right\} dk_h\, d\omega \tag{5.4}$$

It can be checked that when $H = 0$, that is, when we are looking at energy that was propagated with initial takeoff angle $\vartheta_0 = \sin^{-1}(p_0 v_{z=0})$, equation (5.1) becomes $T = 0$. Then equation (5.3) is a *null* operator. This implies that energy propagating with fixed $p = p_0$ will not be moved by the operator T. This property enables velocity estimation at

any depth, consequently with the image of the data itself.

To find the image point we need to insert into equation (5.4) an imaging condition. This condition tell us when the wavefield is an image of the reflectivity. This should happen when we have extrapolated the data to $t = 0$. At this point the energy was reflecting from a given interface. At the reflector the positions of the shot and geophone coordinates should be coincident $s = g$. These imaging conditions translate to $t' = \tau$ in the Snell coordinate system. Substitution into equation (5.4) gives

$$f(h,\tau,t'=\tau) \;=\; \frac{1}{2\pi}\int_{-\infty}^{\infty}\int F(k_h,\tau=0,\omega)\,\exp\left\{ i\int_0^{\tau}\omega\,(T(\xi)-1)\,d\xi + ik_h h \right\} dk_h\,d\omega \quad (5.5)$$

This equation is what we need to image CMP gathers in Snell midpoint coordinates.

Example. Wavefield extrapolation in Snell midpoint coordinates can be illustrated with downward continuation movies. Figures (5.2) and (5.3) show some of the panels calculated for this purpose.

Figure (5.2) is the $p_0 = 0$ case. Downward continuation was done using the phase shift method. Velocity was $v = 1500\ m/s$ with constant τ–steps. As expected, as downward continuation proceeds, energy migrates toward zero–offsets. Past the depth of the reflectors, energy diffracts toward far and negative offsets. Aliased energy (in refractions area) moves in the wrong direction. To image the data, the imaging principle requires collection of energy that is imaged at each downward continuation step.

In figure (5.3) we have the slanted downward continuation situation. For a fixed reflector, energy migrates to the particular offset where the reference Snell wavefront reaches the surface. The LMO correction has the effect of an anti–alias filter. In the slanted frame there is less aliased energy moving in the wrong direction.

6. Wave equation velocity estimation.

Doherty and Claerbout (1976) introduced the wave equation to velocity estimation. The main idea was to downward continue the data to the depth of reflection. At this depth the offset coordinate should be independent of structure, therefore better velocity estimates could be obtained. They also suggested velocity estimation in the ($h = 0$, t, z) plane.

Yilmaz and Chambers (1981) using the wave equation defined a velocity spectrum with equations (5.1) and (5.4) for $p_0 = 0$ by letting velocity v be another variable in the representation:

$$f(h,\tau,t,v) \;=\; \frac{1}{4\pi^2}\int_{-\infty}^{\infty}\int F(k_h,\tau=0,\omega)\,\exp\left\{ iT(v)\,\omega\tau + ik_h h - i\omega t \right\} dk_h\,d\omega \quad (6.1)$$

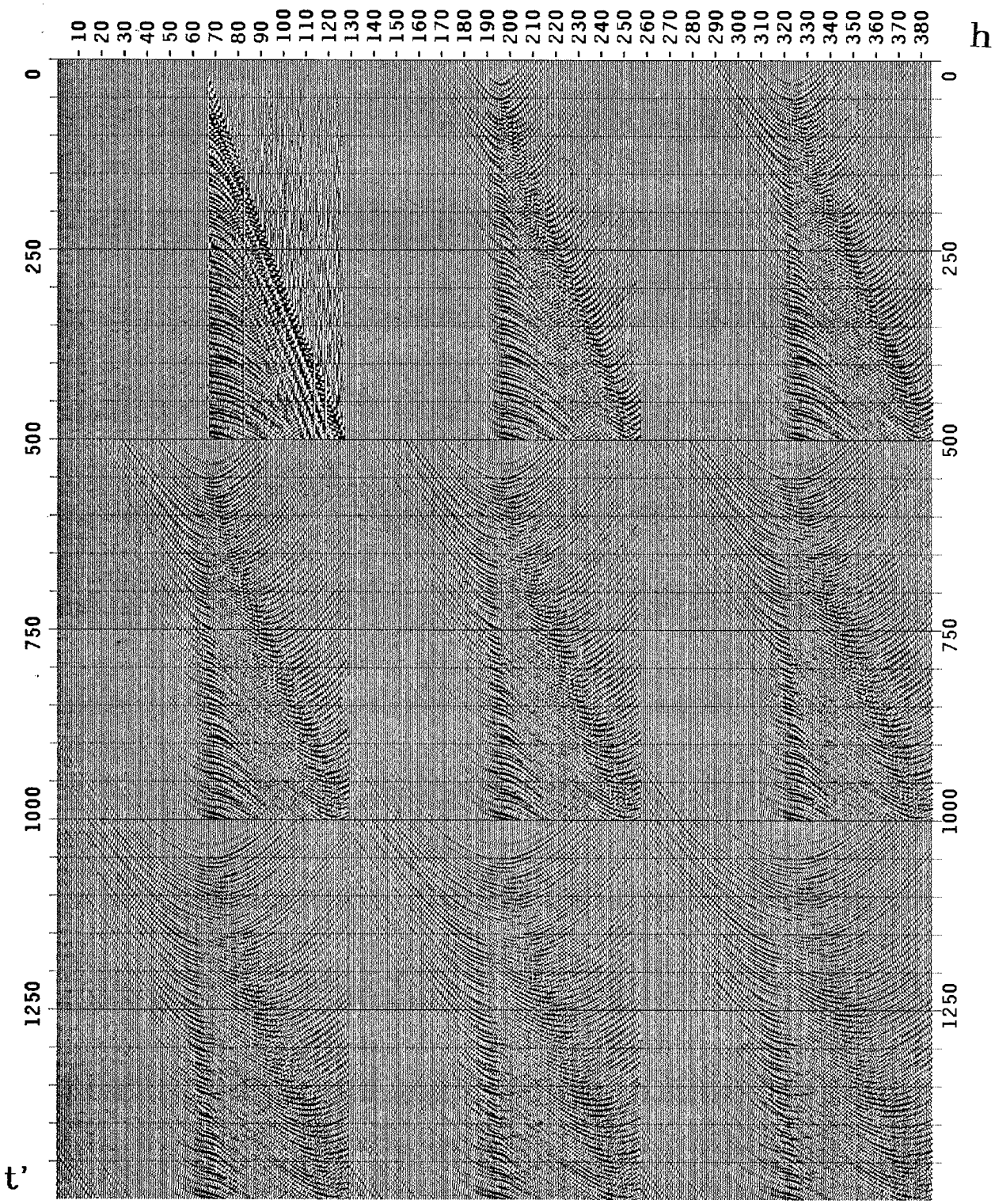

FIG. 5.2. Downward continuation. $p_0 = 0$.

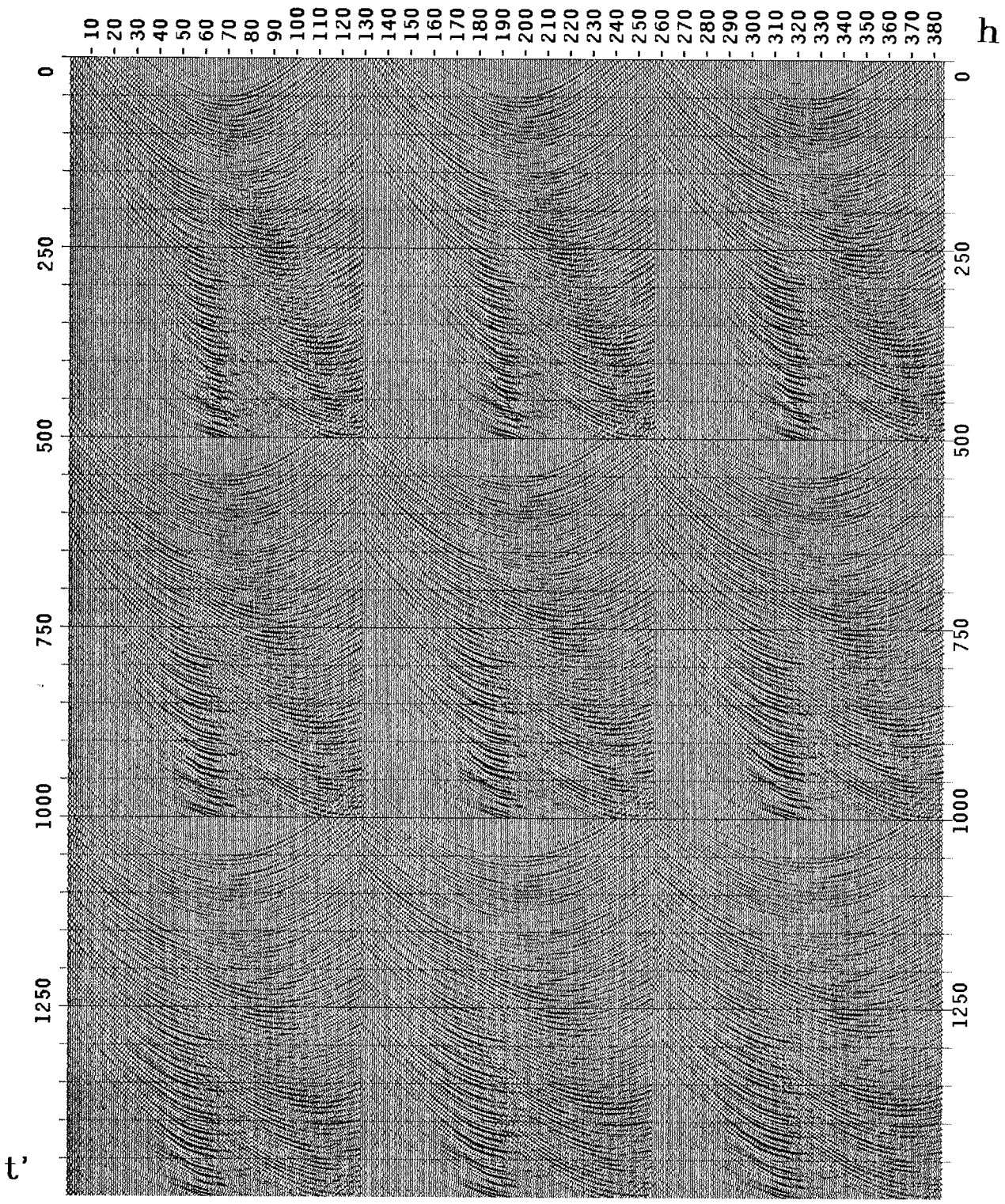

FIG. 5.2. (continuation).

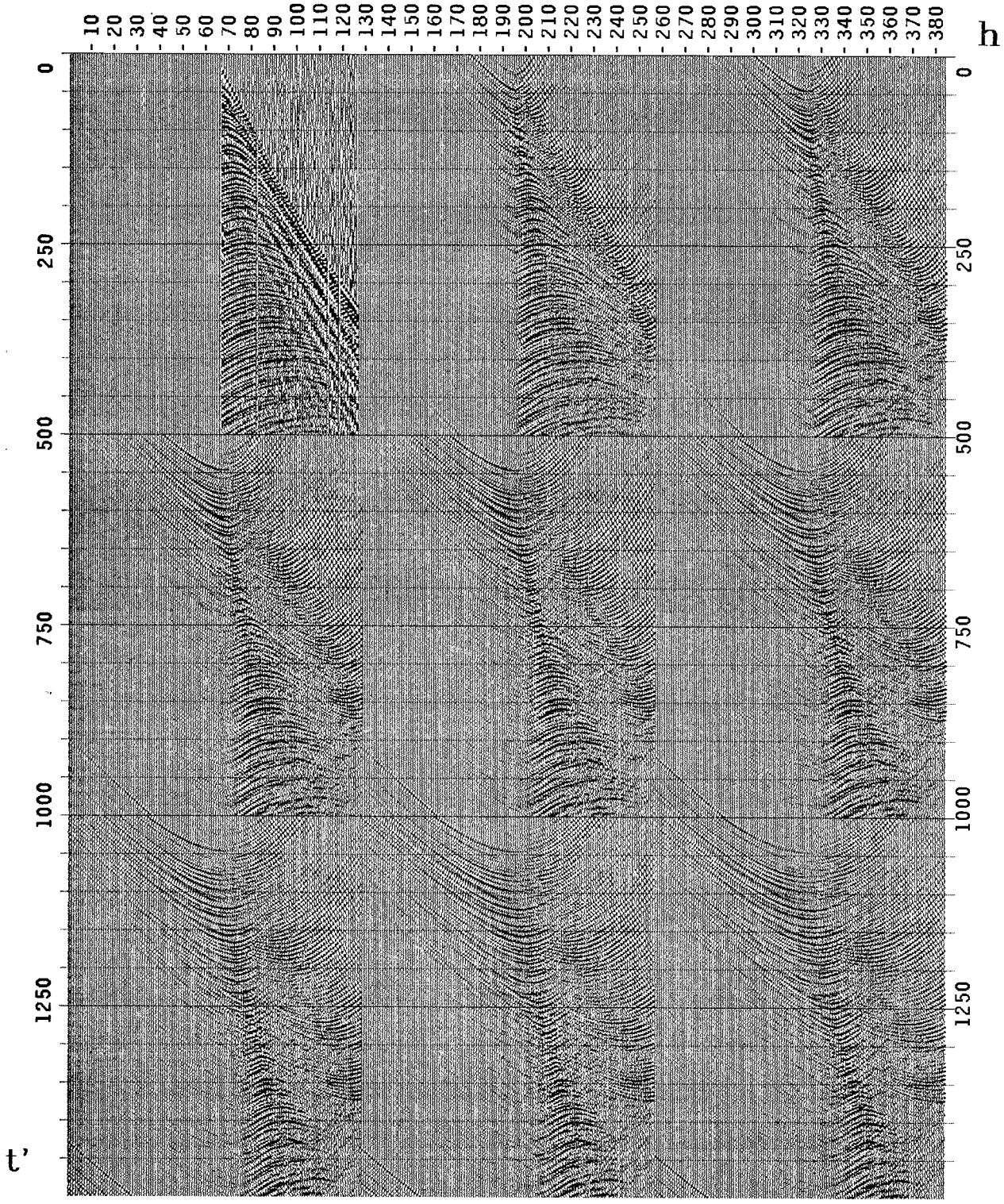

FIG. 5.3. Downward continuation. $p_0 v = 0.3$.

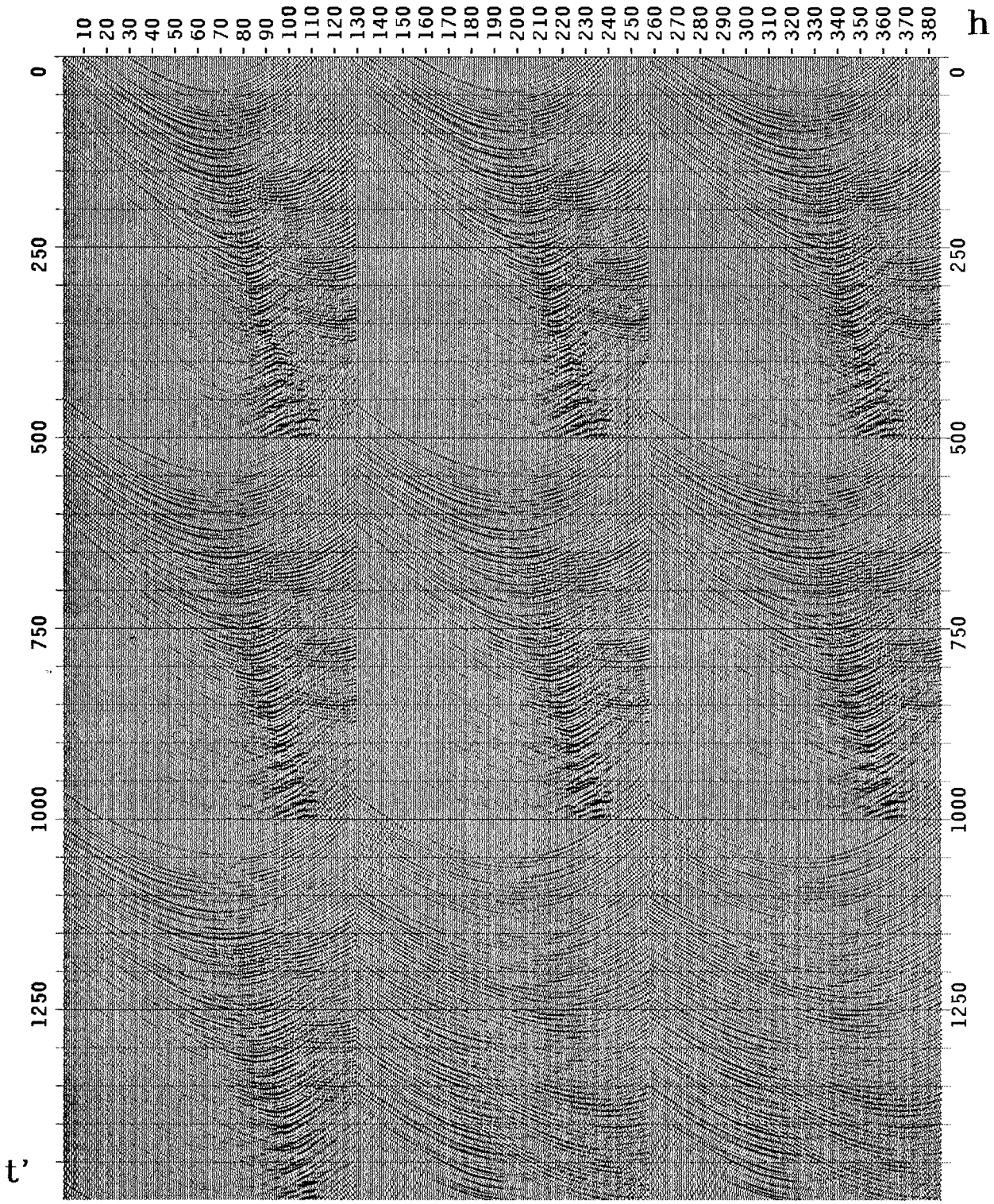

FIG. 5.3. (continuation).

$$T(v) \;=\; 1 - \frac{1}{2}\left[1 - \left(\frac{k_h v}{2\omega}\right)^2\right]^{1/2} \tag{6.2}$$

Their *velocity spectrum* is the plane $f(h=0,\ \tau,\ t=\tau,\ v)$

$$f(h=0,\tau,t=\tau,v) \;=\; \frac{1}{2\pi}\int_{-\infty}^{\infty}\int F(k_h,\tau=0,\omega)\,\exp\left\{i(T(v)-1)\,\omega\,\tau\right\}\,dk_h\;d\omega \tag{6.3}$$

This equation is exact in constant velocity media. In this approach the wave equation stacks the data. The velocity spectrum obtained is similar to Taner and Koehler's (1968).

An alternative approach is to let the wave equation do NMO without stack. This was done by Thorson and Yedlin (1980), and Yedlin and Thorson (1981).

Clayton and McMechan (1981) used iterative wavefield inversion to estimate velocity using post–critical reflections and refraction data.

In section (3) we mentioned how the LMO method had several desirable properties over ray tracing methods of velocity estimation. We proved that the method can be applied at any depth of observation. At the surface of the earth, where data is collected, energy has been diffracted and is non–local. Using the wave equation in Snell midpoint coordinates, we can downward continue the seismic experiment to the depth and offset where the reference slanted wavefront was reflected. At this depth the data is imaged and no wave propagation has taken place. Imaging has the effect of stacking, not to zero offset, but to offsets where reference wavefronts with constant ray parameter p_0 reach the surface. This imaging step adds robustness to the LMO method in a sense of enhancing the signal–to–noise ratio. Cable truncation artifacts are not severe because imaging moves most of the energy inside the data grid.

We define the *linear velocity spectrum* of a CMP gather as its image in Snell midpoint coordinates for a non–vertical reference wavefront. This definition fulfills the requirement that energy be a a local function of velocity. We analyze the resolution of our velocity spectrum while referencing downward continuation algorithms.

Choosing p_0. At some point in the process we need to decide what value of the ray parameter p_0 to use. A large p_0 implies wide propagation angles and increased velocity sensitivity for events with RMS velocity $v \approx 1/p_0$. However, with a large p_0 we cannot estimate high velocities ($v > 1/p_0$). Reference arrivals are beyond the end of the cable. Small p_0 will put low velocity events out of cable too, and since small propagation angles are used, there is a decrease in sensitivity to velocity. When wave equation imaging is used, to avoid severe end effects we also would like to keep a symmetry of positive and negative stepouts. Too small or too large p_0 will enhance the asymmetry of the skewed–hyperbolas

in the data biasing velocity estimates. In practice we probably want to divide the data into several regions with different p_0 according to some rule; for instance

$$p_0 \approx [0.5 - 0.8]/v_{max}$$

But no general rule can be given, the choice of p_0 is data dependent.

Phase shift method. This method is exact up to Nyquist frequencies (wide angles) in stratified media. Exact methods are particularly sensitive to the downward continuation velocity, especially when trying to image wide angle energy. This sensitivity introduces two problems in our application. First, we can only expect to know *a priori* velocity with first order accuracy. Second, even if we know the correct velocity function, the phase shift method will only image primary energy. In some applications the velocity function is multivalued (multiples interfering with primaries), and we would like our velocity spectrum to give as good a resolution as possible for all velocities. The main application we have found for the phase shift method is studying downward continuation in Snell midpoint coordinates.

Stolt method. Stolt's method has the advantage of speed. In a constant velocity medium the method is exact in the propagating region. For velocity estimation it is possible to reduce sensitivity to the background velocity, restricting the range of angles during the imaging step. Limiting the range of angles also makes the method more insensitive to multivalued velocity functions at the expense of blurred images. This is done, remembering that

$$H = \frac{k_h v}{2\omega} = \sin\vartheta'$$

When there are no multiple problems, we can decrease uncertainty in velocity by combining a deformation to hyperbolic space, (SEP–28, p. 103–120) with Stolt's imaging. We start imaging the data with constant velocity for a restricted range of angles, and iterate decreasing the range as uncertainty in the velocity function decreases. (Figure 6.1).

When we apply the iterative process, as the velocity function converges to the true one, Stolt's image aligns itself along the line associated with the backgorund velocity $\hat{v}$ according to equation (3.16). We need a relation to correct the original $\bar{v}(z)$ from the observed departures of the image from $\hat{v}$.

Since from equation (3.3) there is a one–to–one relationship between velocity and the slope $d\tau/dh$ we can write an expansion for the velocity as function of m about $\hat{v}$

$$v = \hat{v} + \left(\frac{dv}{dm}\right)_{v=\hat{v}} \Delta m + \frac{1}{2!}\left(\frac{d^2v}{dm^2}\right)_{v=\hat{v}} (\Delta m)^2 + \cdots \qquad (6.4)$$

where m is equal to the slope $d\tau/dh$.

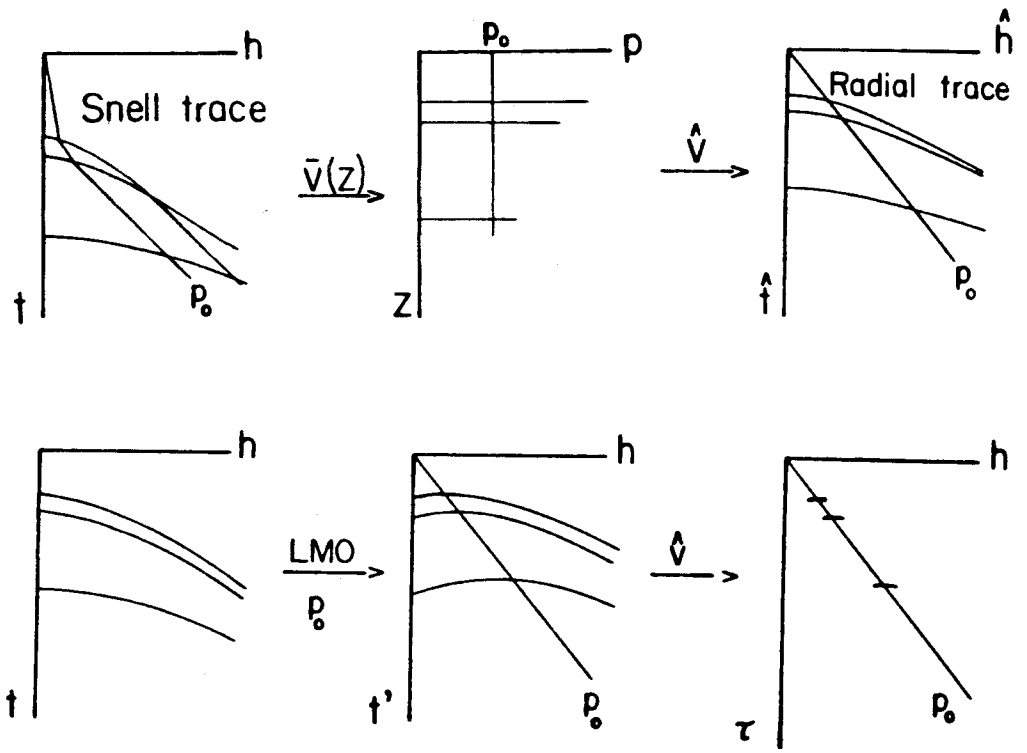

FIG. 6.1. Iterative velocity estimation. Velocity estimation using Stolt imaging and hyperbolic stretch. The process consists of iteratively applying the two steps. Stolt imaging in Snell midpoint coordinates transforms the data into a space where we can read velocities directly from the imaged data. Hyperbolic stretch uses the current velocity function to map the data into a quasi–hyperbolic space. This space is more suitable for Stolt imaging.

We can use equation (3.3) to find $\frac{dv}{dm}$

$$\left(\frac{dv}{dm}\right)_{v=\hat{v}} = -\frac{p_0}{4\left[p_0^2 + \frac{p_0}{2} m_{v=\hat{v}}\right]^{3/2}} \tag{6.5}$$

We also have from (3.3) for $m_{v=\hat{v}}$

$$m_{v=\hat{v}} = 2\,\frac{1-\hat{v}^2 p_0^2}{p_0 \hat{v}^2} \tag{6.6}$$

From these equations we can find the dv correction. Keeping the linear term only

$$dv_{v=\hat{v}} = \bar{v}_{v=\hat{v}} - \hat{v} = \left(\frac{dv}{dm}\right)_{v=\hat{v}} \Delta m = -\frac{p_0 \hat{v}^3}{4}\Delta m \tag{6.7}$$

This is the desired relation.

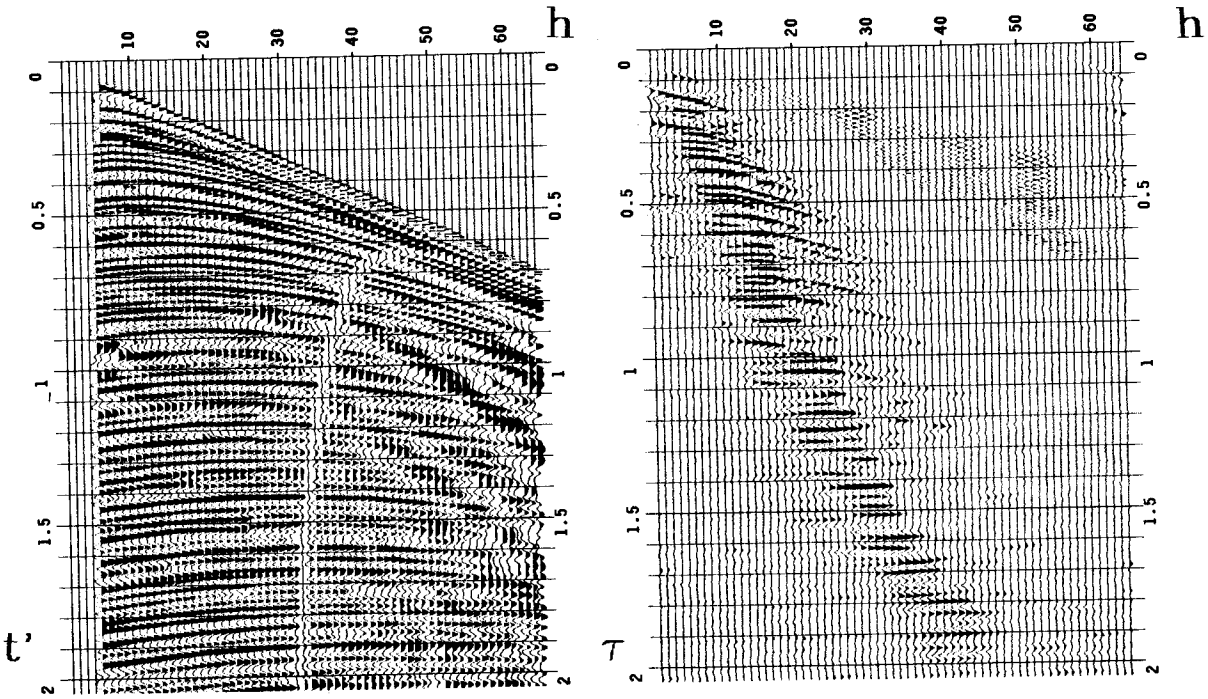

FIG. 6.2. Imaged data in Snell coordinates. (a) Marine CMP gather in Snell midpoint coordinates after hyperbolic deformation. $\bar{v}(z)$ increases linearly with depth from the sea–floor to 1 km. ($\partial v / \partial z = 0.8\ s^{-1}$), (b) Stolt's image, amplitudes squared for display. Most events align along the replacement velocity slope $\hat{v} = 1700\ m/s$. With equation (6.7) we can correct the trial $\bar{v}(z)$ measuring departures from $\hat{v}$. This image defines our *linear velocity spectrum* – now energy is a local function of velocity. ($p_0\hat{v} = 0.255$).

Figure (6.2) shows a field data example of the proposed iterative process. Data was preprocessed with a hyperbolic deformation and subsequently imaged with Stolt's method. In this figure another advantage of the LMO method can be seen, it is always possible to identify the events being used to measure velocity.

Finite difference in (h, τ, ω) domain. Imaging CMP gathers in Snell midpoint coordinates has the useful feature of separating energy with respect to angle. Multiple reflections stay aligned below their associated primaries (at water velocity slope), becoming easier to discriminate. Refractions remain at high angles and do not interfere too strongly with primaries. We would like to exploit this feature in our velocity spectrum.

Fifteen degree finite difference algorithms in (h, τ, ω) space have several advantages. Time derivatives are exact. The fifteen degree equation is insensitive to background velocity within small propagation angles (departures measured from the reference Snell wave propagation angle). In this domain, stepout filtering concurrent with downward continuation is also possible.

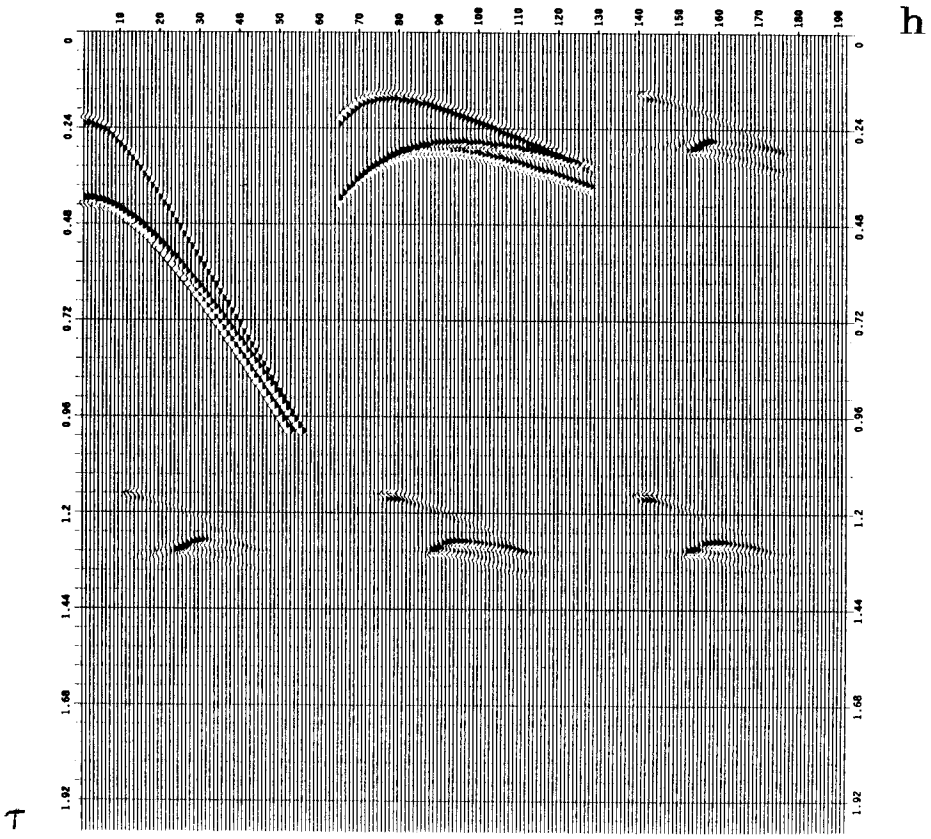

FIG. 6.3. Fifteen degree imaging. Narrow velocity spectrum. (a) Synthetic gather. $v_1 : v_2 : v_3 = 1 : 1 : 1.1$. (b) LMO corrected gather. $p_0 v_1 = 0.725$. (c) Constant velocity $p_0 \bar{v} = 0.80$ imaging. (d) $\bar{v}(h,\tau)$ imaging according to equation (6.9). Velocity was limited to the range $0.75 \leq p_0 \bar{v}(h,\tau) \leq 0.85$. (e) Same as (c) with $w_0 = 8\pi \text{ sec}^{-1}$. (f) Same as (d) with $w_0 = 8\pi \text{ sec}^{-1}$. Images have been squared for display. When trying to resolve narrow velocity variations, we want p_0 close to $1/v_m \, a\, x$, and small variations in the downward continuation velocity. Compare (c) with (d) and (e) with (f). There is a visible effect out of using $v(h,\tau)$, even though it varied only 6.25 % from the mean.

Since our equations are now in offset space, the possibility of allowing variations of velocity with offset is open. This may help contravene numerical dispersion errors. More important, from equation (6.3) we know that Snell wave arrival positions are function of velocity. For a fixed τ we expect to see low velocity arrivals at offsets smaller than fast velocity arrivals. Keeping in mind that the fifteen degree approximation correctly images the Fresnel zone of a given reflection, it should be able to handle multi-valued velocity functions. When there are two simultaneous arrivals at zero offset in the data, this would happen if the Fresnel zone of both reflectors decouples within cable boundaries at large offsets. We could then use low velocities at small offsets and high velocities at large

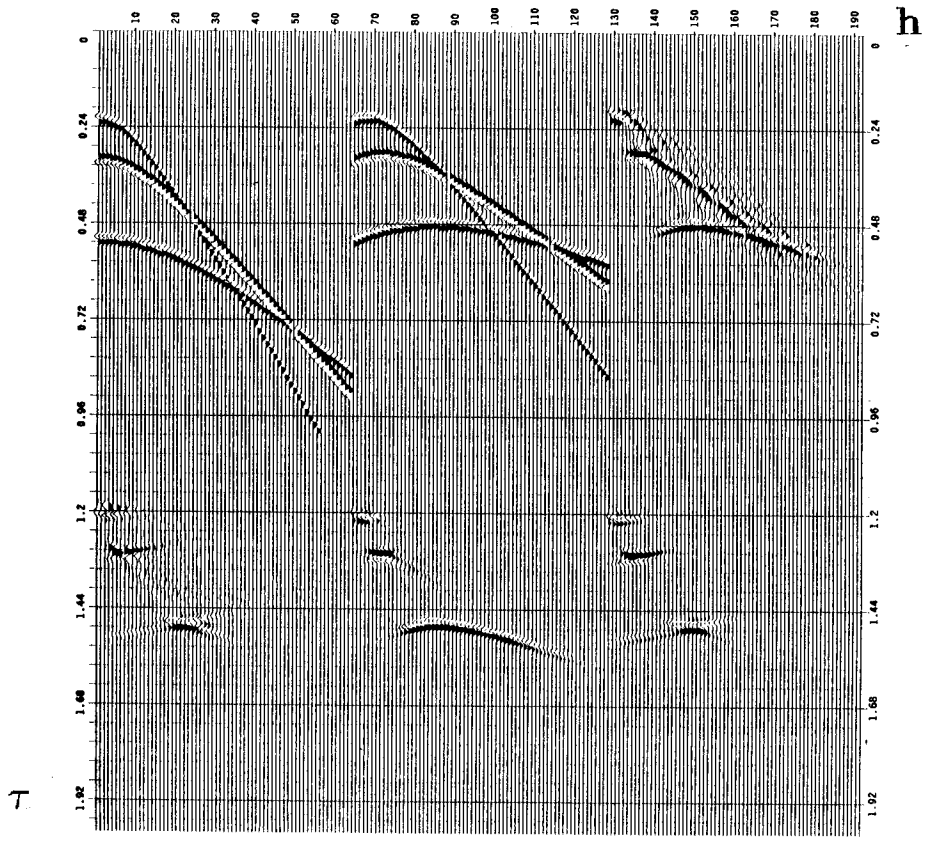

FIG. 6.4. Fifteen degree imaging. Wide velocity spectrum. (a) Synthetic gather. $v_1 : v_2 : v_3 = 1 : 1.5 : 2$. (b) LMO corrected gather. $p_0 v_3 = 0.5$. (c) Constant velocity $p_0 \bar{v} = 0.35$ imaging. (d) $\bar{v}(h,\tau)$ imaging according to equation (6.9). Velocity was limited to the range $0.175 \leq p_0 \bar{v}(h,\tau) \leq 0.525$. (e) Same as (c) with $w_0 = 8\pi$ sec^{-1}. (f) Same as (d) with $w_0 = 8\pi$ sec^{-1}. Images have been squared for display. $v(h,\tau)$ has a broad range of variation for this application. We get a sharper image when using inhomogeneous instead of constant downward continuation velocity.

offsets. When chosing p_0 these arguments should be kept in mind. Energy outside the Fresnel zone can be filtered out.

The fifteen degree equation in Snell midpoint coordinates is given by

$$\frac{\partial}{\partial \tau} f(h,\tau,\omega) = \frac{v(h,\tau)^2}{8(w_0 - i\omega)\left[1 - p_0^2 v(h,\tau)^2\right]} \frac{\partial^2}{\partial h^2} f(h,\tau,\omega) \tag{6.8}$$

where w_0 is the stepout filtering parameter.

For a choice of $v(h,\tau)$ we can use equation (3.3) as

$$v^2(h,\tau) = \frac{1}{p_0\left[p_0 + \frac{1}{2}\frac{\tau}{h}\right]} \tag{6.9}$$

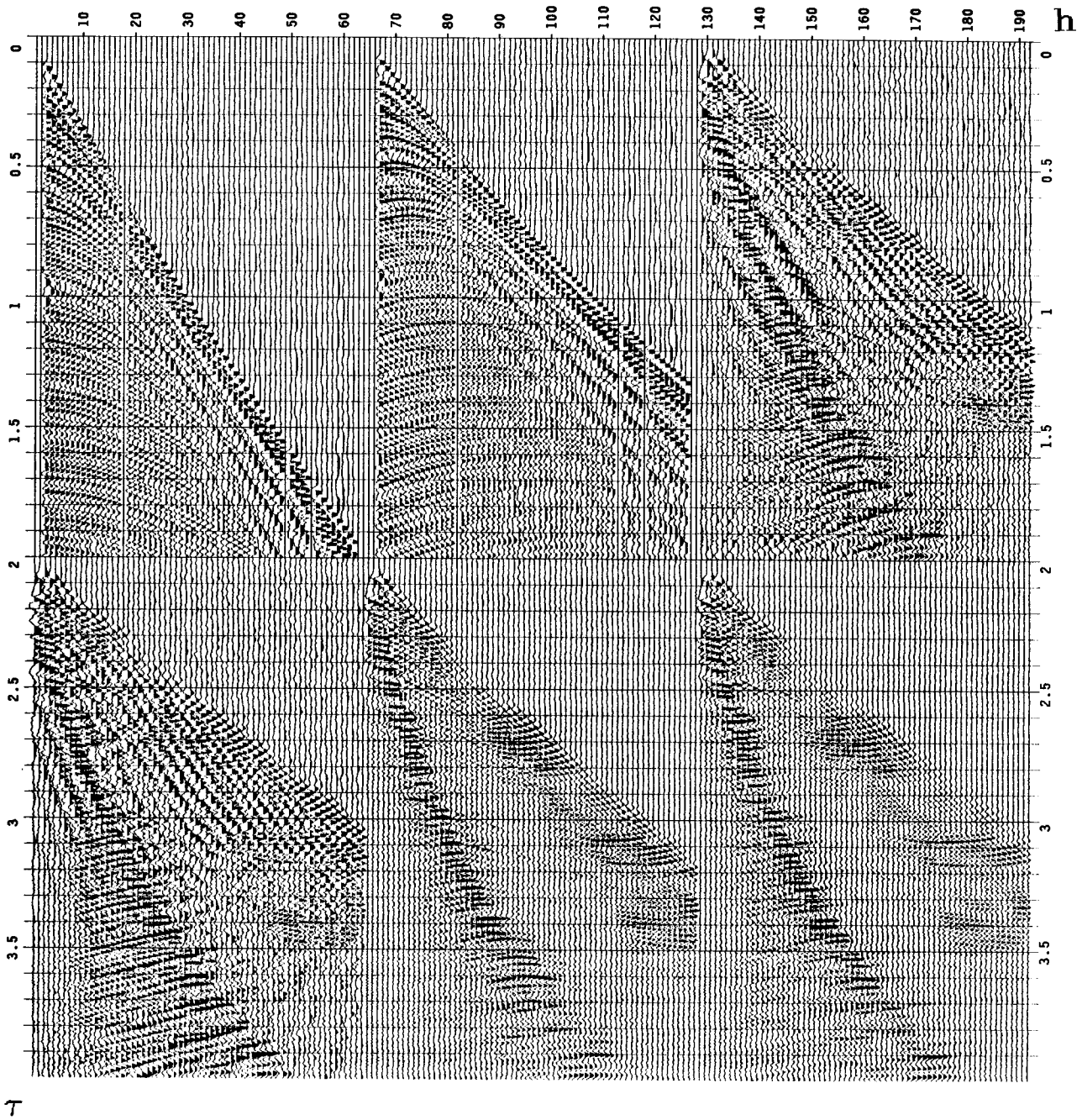

FIG. 6.5. Fifteen degree imaging. Field data example. Wide velocity spectrum. (a) CMP gather. (b) LMO gather $p_0 = 1/5000\ sec/m$. (c) Constant velocity imaging. $\bar{v} = 2000\ m/sec$. (d) $v(h,\tau)$ imaging. Velocity was allowed to vary with offset according to equation (6.9) in the range $1200\ m/sec \le \bar{v} \le 2800\ m/sec$. (e) Same as (c) with $w_0 = 8\pi\ \text{sec}^{-1}$. (f) Same as (d) with $w_0 = 8\pi\ \text{sec}^{-1}$. This data set has strong multiple refractions that give strong interference with the image in both constant and variable velocity imaging. With constant velocity imaging the image is not well defined for the first second of data. Variable velocity defines it better. However variable velocity has strong unmigrated high stepout events in the low velocity zone. With stepout filtering is added, the quality of the image is slightly better when $v(h,\tau)$ was used.

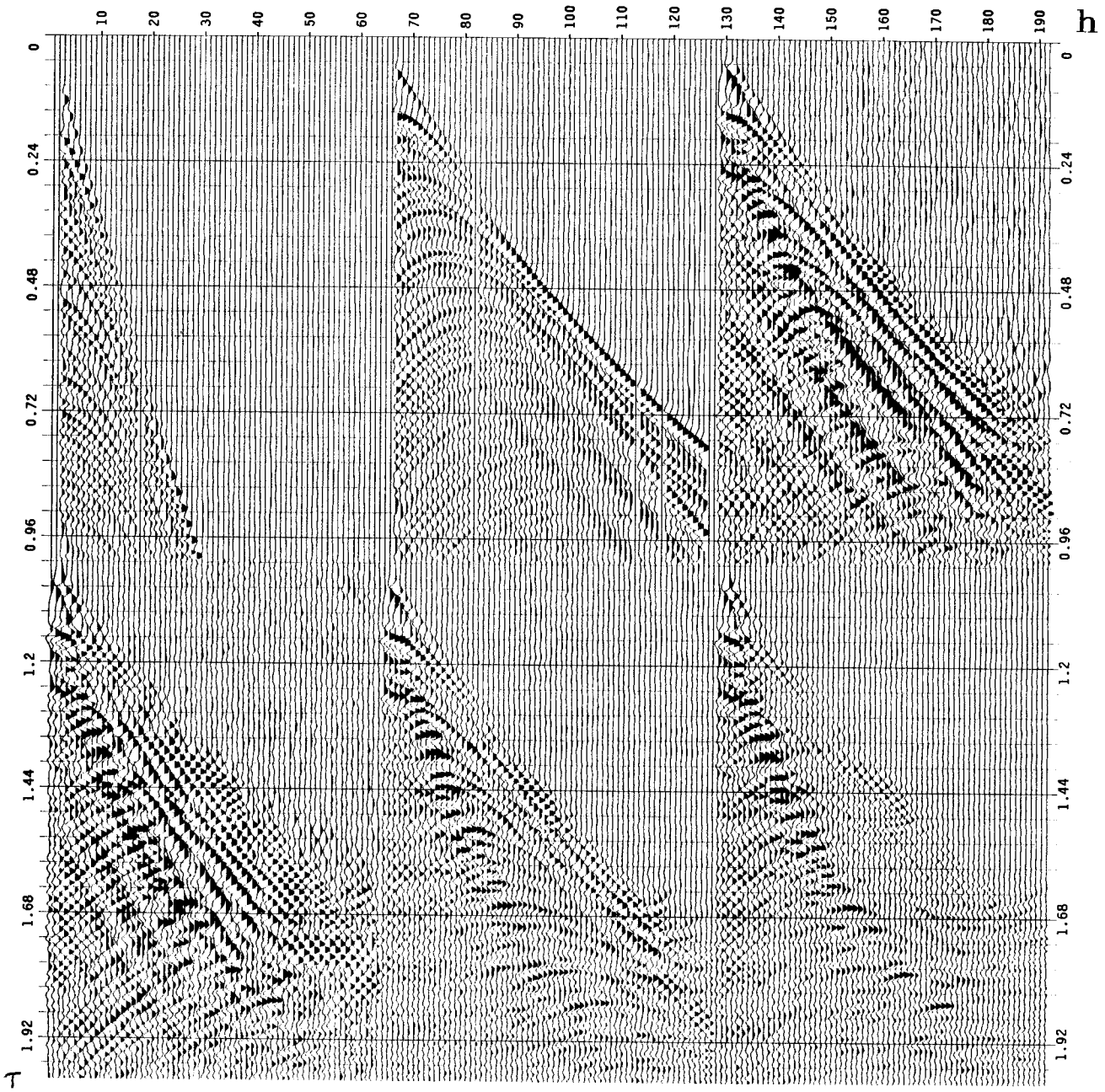

FIG. 6.6. Fifteen degree imaging. Field data example. Narrow velocity spectrum. (a) CMP gather. (b) LMO gather $p_0 = 1/2667\ sec/m$. (c) Constant velocity imaging. $\bar{v} = 1800\ m/sec$. (d) $v(h,\tau)$ imaging. Velocity was allowed to vary with offset according to equation (6.9) in the range $1400\ m/sec \le \bar{v} \le 2200\ m/sec$. (e) Same as (c) with $w_0 = 8\pi\ \text{sec}^{-1}$. (f) Same as (d) with $w_0 = 8\pi\ \text{sec}^{-1}$. For this window of data, multiple refractions interfere severly with the image of the data. Imaging without numerical viscosity does not give good resolution. Stepout filtering and $v(h,\tau)$ improve the image quality. In (f) the spectrum has resolved peg–leg multiples aligned at water slope. They image below primary arrivals.

Figure (3.1) shows how this equation dictates the velocity distribution in (h, τ) space.

In the fifteen degree equation (6.8) $v(h, \tau)$ is expected to be an interval velocity, while equation (6.9) defines RMS velocities. The fifteen degree equation is insensitive to this distinction. To justify the use of equation (6.9), consider an event at time–depth τ. We need to extrapolate τ sec to reach the depth of the event. Assuming only τ dependence in velocity*, the coefficient of equation (6.8) from its finite difference scheme is

$$a(\tau) \equiv \frac{v^2(\tau)\,\Delta\tau}{16\,\omega[\,1 - p_0^2\,v^2(\tau)\,]\,\Delta h^2} \tag{6.10}$$

The cumulative effect of downward continuation is given by the integral

$$\int_0^\tau a(\xi)\,d\xi = \frac{\Delta\tau}{16\,\omega\,\Delta h^2} \int_0^\tau \frac{v^2(\xi)}{1 - p_0^2\,v^2(\xi)}\,d\xi \tag{6.11}$$

we recognize the v_{RMS} expression of equation (3.13); define $\bar{a}$ as

$$\bar{a} \equiv \frac{1}{\tau}\int_0^\tau a(\xi)\,d\xi = \frac{\Delta\tau}{16\,\omega\,\Delta h^2}\,\frac{v_{RMS}^2}{1 - p_0^2\,v_{RMS}^2} \tag{6.12}$$

Therefore with the fifteen degree equation there is no difference in extrapolating a single τ step with $\bar{a}$ or extrapolating continuously with $a(\tau)$. This insensitivity was exploited to estimate velocity in the $(h = 0, t, z)$ plane for $p_0 = 0$ by Doherty and Claerbout (1974). Unfortunately their analysis cannot be extended to $p_0 \neq 0$. The plane $(h = h_0, t, z)$ where energy focuses is velocity dependent. In addition, this plane is non–unique when velocity is multivalued.

Figure (6.3) is an example of imaging to resolve two simultaneous arrivals. The synthetic shows to events with RMS velocities differing by 5%. The reference ray parameter should be chosen so the stationary region of LMO corrected events separates according to velocity. We also need to restrict the range of variation of the downward continuation velocity. The figure illustrates a problem trying to get an image with large p_0. When the energy distribution is not symmetric with stepout, the maximum cluster of energy will migrate as downward continuation proceeds. When imaging, the maximum–energy locations will not necessarily coincide with the stationary location of events, this can result in a bias estimating velocity. Stepout filtering partially solves this problem.

Figure (6.4) is an example of imaging to resolve wide velocity variations. In this application the range of variations of $v(h, \tau)$ is broader than in the previous example. Imaging gives a sharper focus when $v(h, \tau)$ is used instead of constant downward continuation

*In the neighborhood where the fifteen degree wave equation is valid $v(h, \tau) \approx v(\tau)$.

velocity.

Figure (6.5) is an example with field data. The spectrum is obtained for two seconds of data. The data set has particularly strong multiple refractions. The image illustrates how the LMO method separates events with velocity. Refractions remain at large offsets and can easily be removed with stepout filtering, this way they will not interfere in the velocity estimation process. Figure (6.6) is the example with the first second of data. The filtered image is better when $v(h,\tau)$ is used. Some pegleg multiples have been resolved.

7. Conclusions.

In this chapter we have defined a linear velocity spectrum as the image of a CMP gather in Snell midpoint coordinates for a non–vertical Snell reference wave. This definition fulfills most requirements of a velocity spectrum. 1) It is obtained through linear transformations in the data. 2) Energy distribution is a local function of velocity. 3) Velocity estimation can be done with any slanted reference Snell wave. 4) Interval and RMS velocities are measured directly in the data. 5) Cable truncations and refractions do not severly impair resolution. Also, unlike semblance techniques, it is easy to identify the events used to get the velocity function. The spectrum is flexible, the choice of the reference Snell wave could be done to suit the particular data set of interest. When several reference Snell waves are used, the LMO method can be used to quantify the effect of velocity variations between reflectors in the interval velocity estimates. For computation, Stolt's method is fast and can be combined with a hyperbolic deformation to sharpen the image. The fifteen degree wave equation in offset space is particularly useful since $v(h,\tau)$ can be used to resolve multi–valued velocity functions. We do not need *a priori* knowledge of velocity. The method is sensitive to aliasing, but the LMO correction partially solves the problem. All these properties make the spectrum attractive, not only for velocity estimation but in applications demanding a data space satisfying linearity and locality requirements.

ACKNOWLEDGMENT

Rick Ottolini wrote the hyperbolic semblance velocity program. The data set was kindly provided by CONOCO to SEP.

REFERENCES

Claerbout, J.F., 1980, Lecture notes. Stanford Exploration Project, v. 25, p. 185–361.

Clayton, R.W., and McMechan, G.A., 1981, Inversion of refraction data by wavefield continuation: Geophysics, v. 46, p. 860–868.

Diebold, J.B., and Stoffa, P.L., 1981, The traveltime equation. tau-p mapping and inversion of common midpoint data: Geophysics, v. 46, p. 238–254.

Dix, C.H., 1955, Seismic velocities from surface measurements: Geophysics, v. 20, p. 68–86.

Doherty, S.M., and Claerbout, J.F., 1974, Velocity estimation based on the wave equation: Stanford Exploration Project, v. 1, p. 160–178.

Doherty, S.M., and Claerbout, J.F., 1976, Structure independent velocity estimation: Geophysics, v. 41, p. 850–881.

Green, C.H., 1938, Velocity determinations by means of reflection profiles: Geophysics, v. 3, p. 295–305.

Hajnal, Z., and Serada, I.T., 1981, Maximum uncertainty of interval velocity estimates: Geophysics, v. 46, p. 1543–1547.

LePichon, X., Ewing, J., and Houtz, R.E., 1968, Deep–sea sediment velocity determination made while reflection profiling: J. Geophys. Res., v. 73, p. 2597–2613.

May, B.T., and Straley, D.K., 1979, Higher–order moveout spectra: Geophysics, v. 44, p. 1193–1207.

Neidell, N.S., and Taner, M.T., 1971, Semblance and other coherency measures for multichannel data: Geophysics, v. 36, p. 482–497.

Schultz, P.S., 1981, Method for direct estimation of interval velocities in the near surface: Geophysics, v. 46, p. 419. (Abstract).

Taner, M.T., and Koehler, F., 1969, Velocity spectra, digital computer derivation and applications of velocity functions: Geophysics, v. 34, p. 859–881.

Thorson, J.R., and Yedlin, M.J., 1980, Wave equation moveout: Stanford Exploration Project, v. 25, p. 69–79.

Yedlin, M.J., and Thorson, J.R., 1981, Wave equation moveout, PartII: Stanford Exploration Project, v. 26, p. 107–111.

Yilmaz, O., and Chambers, R.E., 1981, Velocity analysis by wave field extrapolation: Geophysics, v. 46, p. 418. (Abstract).